Supporting Information

Flexible large-area graphene films of 50-600 nm-thickness with high carrier mobility

Shiyu Luo[1], Li Peng[1,2], Yangsu Xie[3], Xiaoxue Cao[1], Xiao Wang[4], Xiaoting Liu[1], Wenzhang Fang[1], Tingting Chen[3], Zhanpo Han[2], Peidong Fan[5], Haiyan Sun[5], Ying Shen[1], Fan Guo[1], Yuxing Xia[1], Kaiwen Li[1], Xin Ming[1], Chao Gao[1]**

[1]MOE Key Laboratory of Macromolecular Synthesis and Functionalization, Department of Polymer Science and Engineering, Zhejiang University, Hangzhou 310027, China.

[2]ZJU-Hangzhou Global Scientific and Technological Innovation Center, School of Micro-nanoelectronics, Zhejiang University, Hangzhou 310027, China.

[3]College of Chemistry and Environmental Engineering, Shenzhen University, Shenzhen, Guangdong 518055, China.

[4]Shenzhen Key Laboratory of Nanobiomechanics, Shenzhen Institute of Advanced Technology, Chinese Academy of Sciences, Shenzhen 518055, China.

[5]Hangzhou Gaoxi Technol Co Ltd, Hangzhou 311113, China.

* Corresponding author. E-mail: Li Peng (l-peng@zju.edu.cn)

Chao Gao. (chaogao@zju.edu.cn)

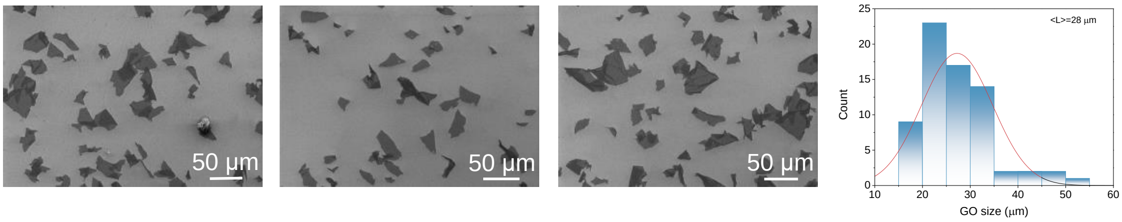

Figure S1. SEM images and lateral size distribution of GO sheets.

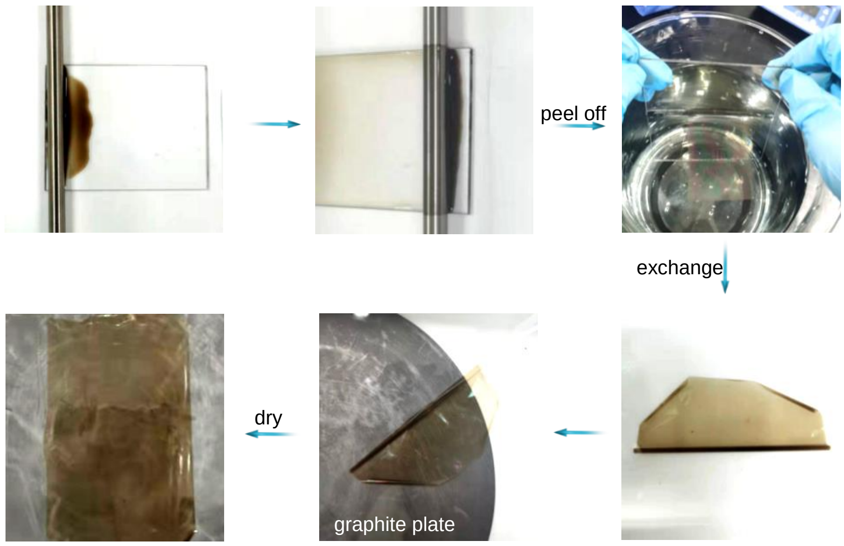

Figure S2. The preparation process of free-standing GO/PAN film.

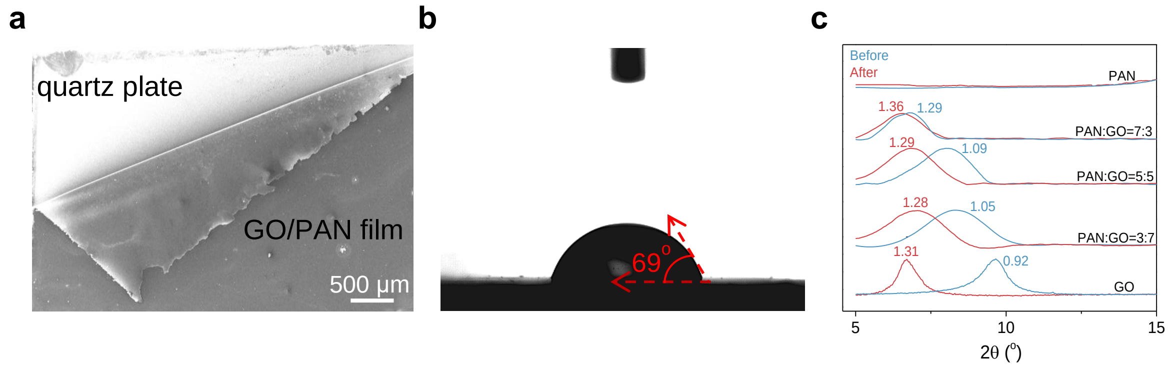

Figure S3. (a) SEM image of GO/PAN film exfoliated by water. (b) The water contact angle of the quartz plate. (c) XRD patterns of GO/PAN films with different PAN contents before and after swelling by water (unit: nm).

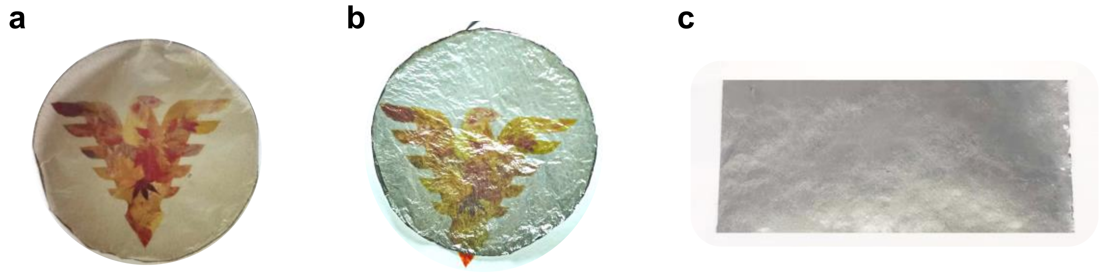

Figure S4. 50 nm-thick nMAG with a round shape before (a) and after (b) 3000 °C heat treatment. (c) 600 nm-thick nMAG with a rectangle shape after 3000 °C heat treatment.

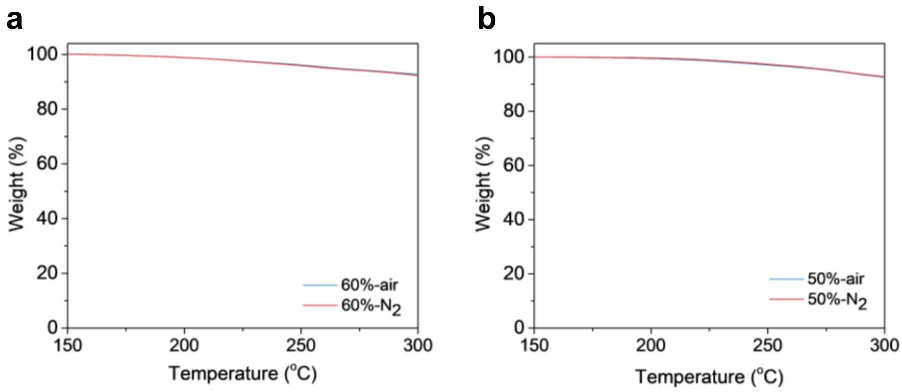

Figure S5. (a) TGA plot of GO/PAN (PAN, 60%) in N_2 and air atmosphere at 150–300 °C. (b) The TGA plot of GO/PAN (PAN, 50%) in N_2 and air atmospheres at 150–300 °C.

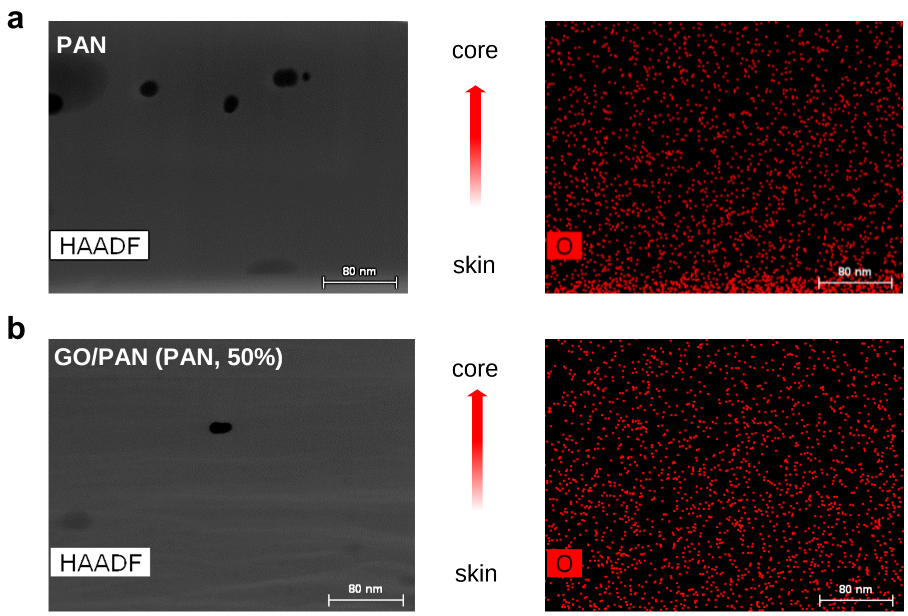

Figure S6. Cross-sectional STEM image of (a) PAN and (b) GO/PAN (PAN, 50%) after pre-oxidation at 270 °C and the corresponding oxygen EDS mapping image, indicating a "skin-core structure" in PAN.

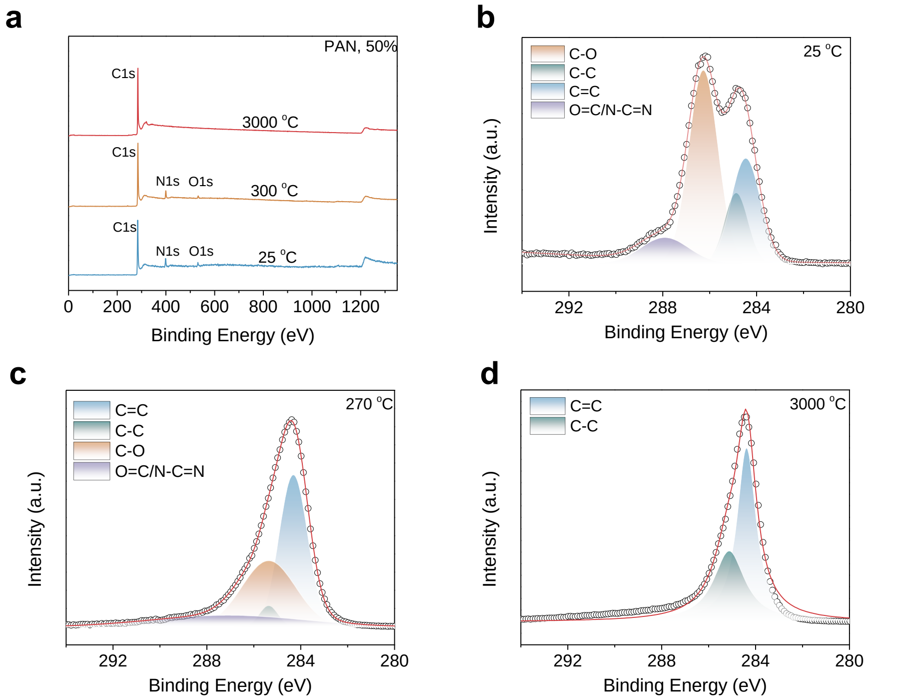

Figure S7. (a) XPS surveys of the nMAG (PAN, 50%) with different heat treatments. (b-d) XPS C1s spectra of the nMAG (PAN, 50%) with different heat treatments, respectively. The circles are experimental data, and the red line is the fitted curve.

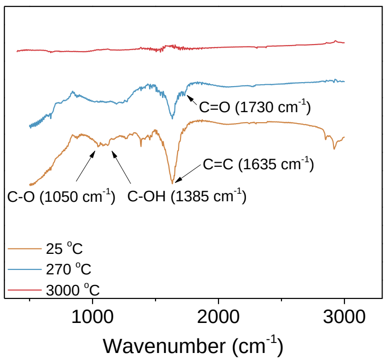

Figure S8. The FTIR spectra of nMAG (PAN, 50%) with different heat treatments.

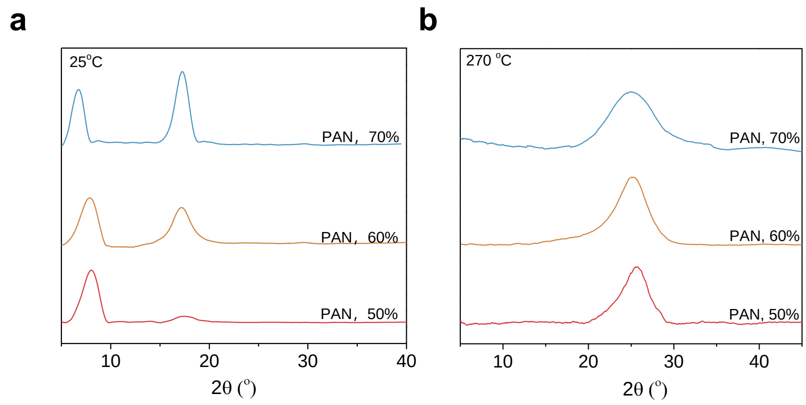

Figure S9. XRD patterns of GO/PAN films before (a) and after (b) pre-oxidation.

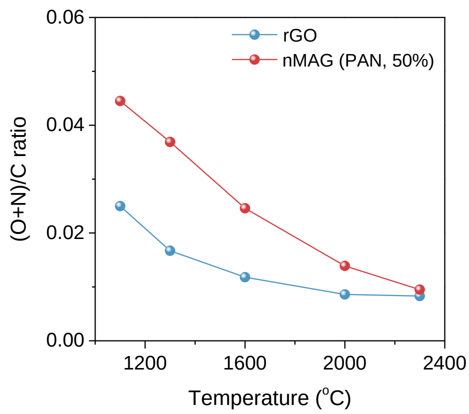

Figure S10. (O+N)/C ratios of rGO and nMAG (PAN, 50%) elaborated by XPS.

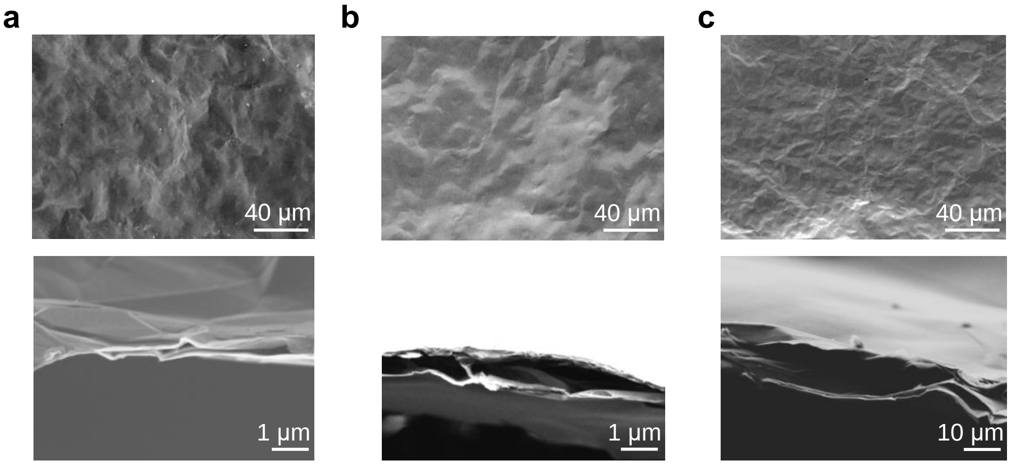

Figure S11. (a) Surface and cross-sectional SEM images of 250 nm-thick nMAG (PAN content, 50%). (b) Surface and cross-sectional SEM images of 450 nm-thick nMAG (PAN content, 60%). (c) Surface and cross-sectional SEM images of 650 nm-thick nMAG (PAN content, 70%).

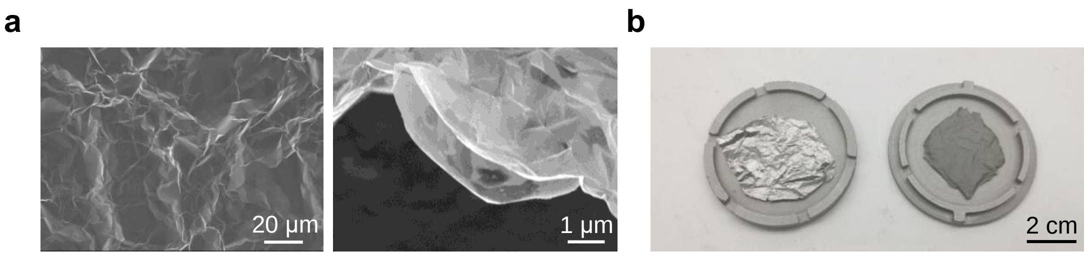

Figure S12. (a) Surface and cross-sectional SEM images of 50 nm-thick GO-based graphene nanofilm obtained by vacuum-filtration. (b) Digital photo of nMAG (PAN, 50%, left) and GO-based graphene nanofilm (right) with the same thickness of 200 nm after heat treatment at 3000 ^{o}C.

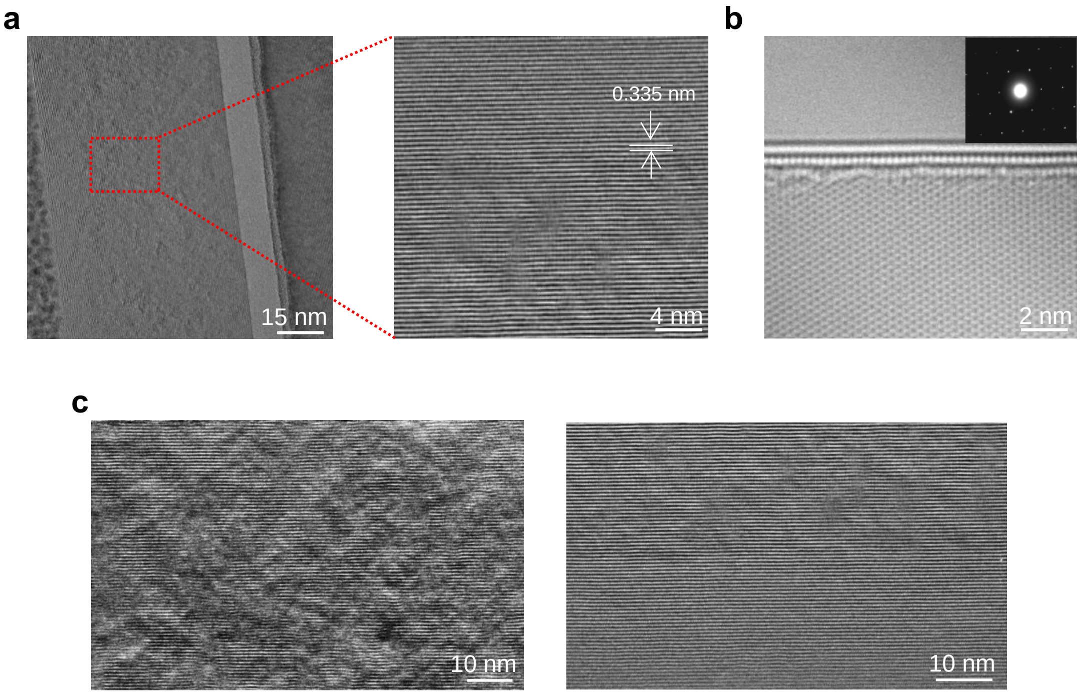

Figure S13. (a) Cross-sectional TEM image of 50 nm-thick nMAG with a graphite-like *d*-spacing. (b) Surface High-Resolution TEM image of graphene sheets in 50 nm-thick nMAG with perfect in-plane lattice and the corresponding selected area electron diffraction pattern (inset), which indicates an AB stacking geometry. (c) Cross-sectional TEM images of nMAG with parallel graphene lattices.

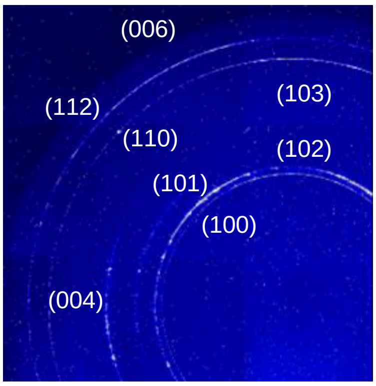

Figure S14. 2D synchrotron WAXS patterns of 50-thick nMAG treated under 3000 ^{o}C.

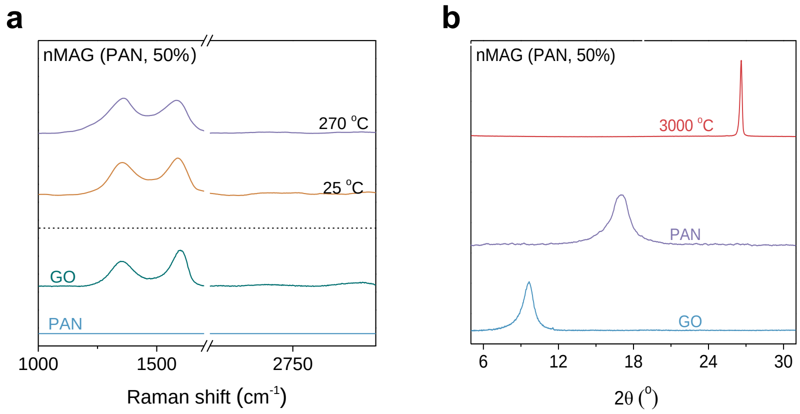

Figure S15. (a) Raman spectra of GO, PAN, GO/PAN (PAN, 50%), and 270 °C-treated GO/PAN (PAN, 50%) films. (b) XRD patterns of GO, PAN, and 3000 °C-treated nMAG.

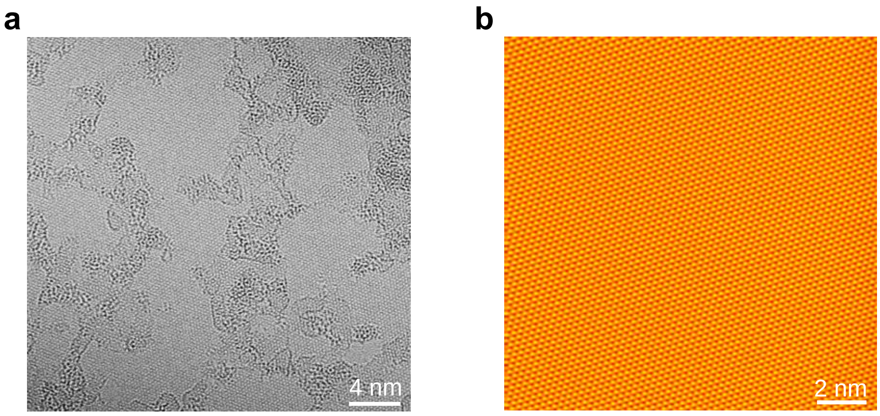

Figure S16. (a) HR-TEM image of GO. (b) STM images of 50 nm-thick nMAG surface.

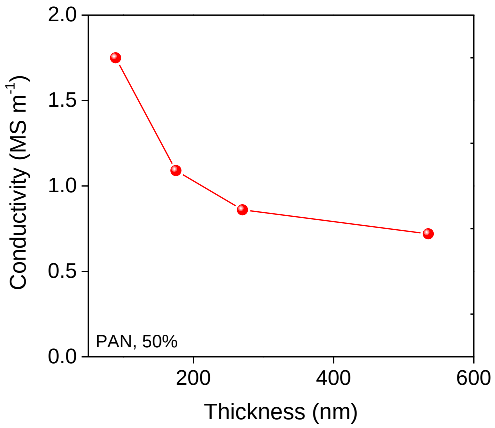

Figure S17. Electronic conductivity of HI-reduced GO/PAN films of different thicknesses (PAN, 50%) heat-treated at 3000 °C.

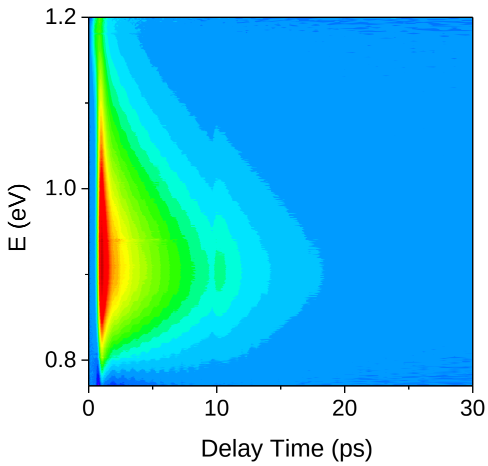

Figure S18. 2D transient absorption map of nMAG/Si as a function of delay time and incident photon energy.

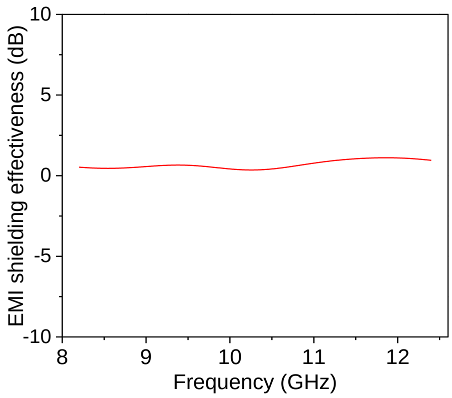

Figure S19. EMI SE_T of PI substrate in the frequency range of 8.2-12.4 GHz.

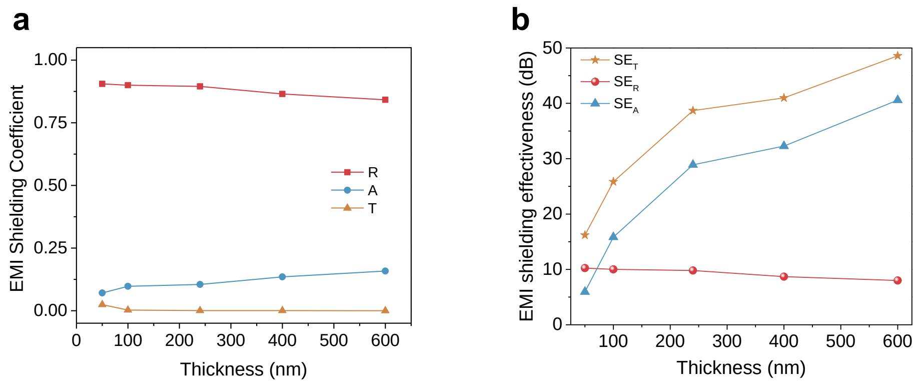

Figure S20. (a) Calculated EMI shielding coefficients of nMAGs in the X-band. (b) SE_R, SE_A, and SE_T values of nMAGs with different thicknesses of 50 nm, 100 nm, 240 nm, 400 nm, and 600 nm in the X-band.

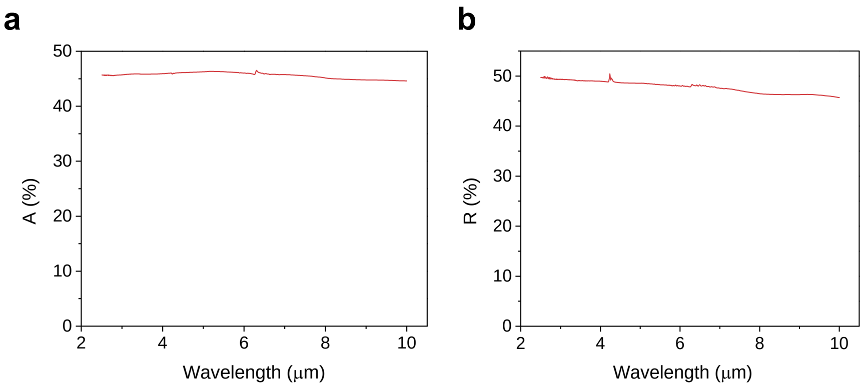

Figure S21. Fourier transform infrared (FTIR) absorption spectrum (a) and reflection spectrum (b) of 50 nm-thick nMAG.

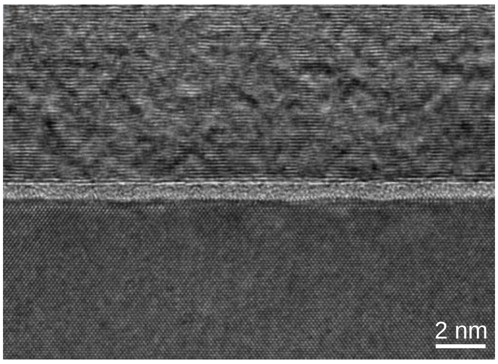

Figure S22. High-Resolution TEM image of nMAG/Si cross-section.

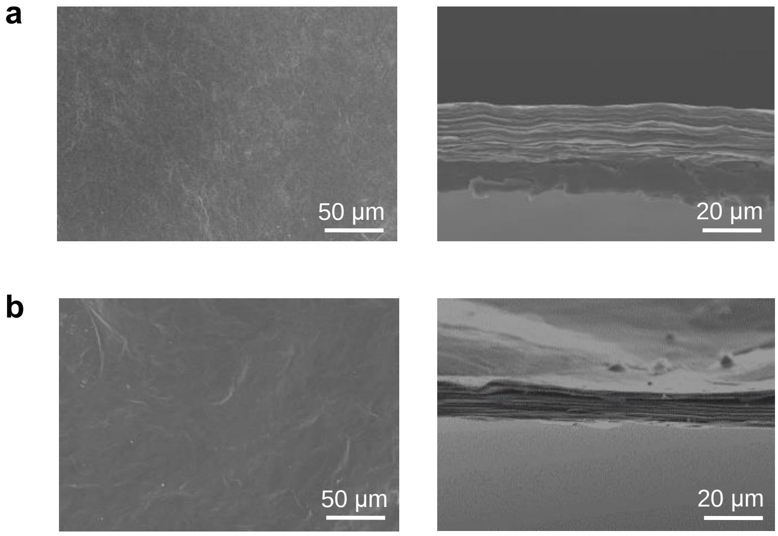

Figure S23. Surface and cross-sectional SEM images of mMAG heat-treated under (a) 270 ^{o}C and (b) 3000 ^{o}C.

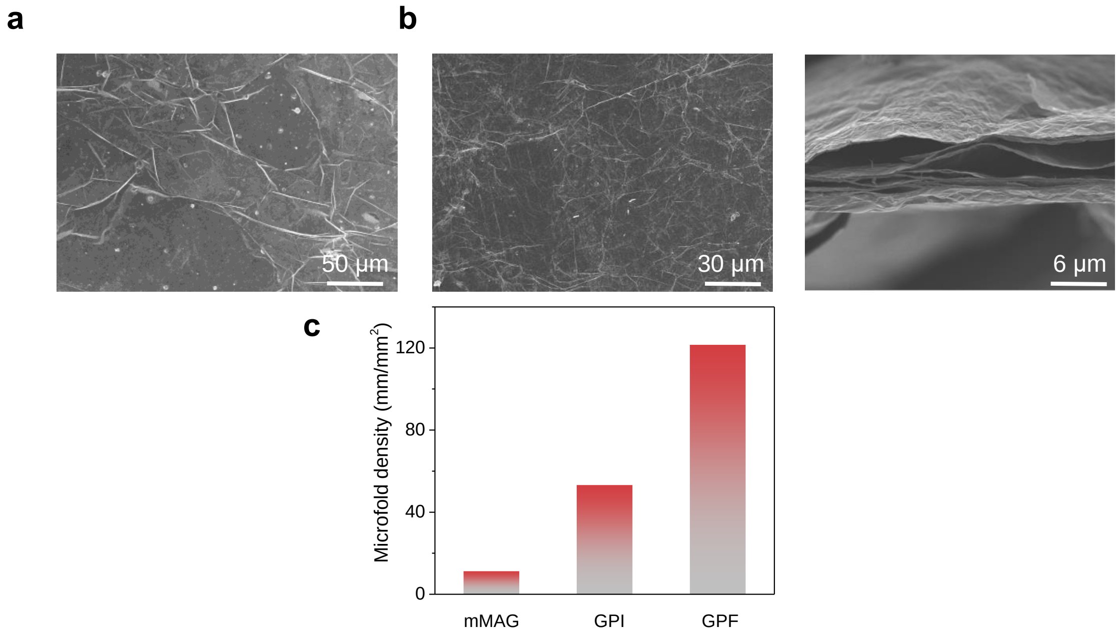

Figure S24. (a) Surface SEM image of commercial artificial PI-based graphite film (GPI). (b) Surface (left) and cross-sectional (right) SEM images of 10 μm-thick GPF (direct scraping of GO/PAN solution). (c) The microfold density of mMAG, GPI, and GPF films.

Table S1. The thicknesses of GO/PAN films with different mass ratios after pre-oxidation and heat treatment at 3000 °C.

GO:PAN (wt%:wt%)	50%:50%	40%:60%	30%:70%
pre-oxidation	421 nm	872 nm	1590 nm
3000 °C treatment	243 nm	400 nm	594 nm

Table S2. The detachment results in different composite films with 2D sheet and polymer, which is detached (√) or not detached (×).

	PAN	Sodium lignin sulfonate
GO	√	×
rGO	×	√

Table S3. Electrical conductivity of the graphite film made from high-temperature thermal treatment.

Material	Thickness (nm)	Conductivity (M S m^{-1})	Temperature (°C)	Ref.
Carbon Films	480	1.7	1400	1
Graphite film	54	1.81	2800	2
Graphene film	48	1.8	3000	3
Graphite Film	77	0.26	1200	4
Graphene film	10000	0.11	2800	5
Graphene film	10000	1.06	3000	6
Graphite Film	25000	1.1	2850	7
Graphene Film	2700	0.1	2000	8
This work	50	2.04	3000	

Table S4. EMI shielding performances of various EMI materials.

	Materials	Thickness [μm]	Density [g cm^{-3}]	SE [dB]	SSE/t [dB cm^2 g^{-1}]	Ref.
graphene	Graphite film	0.231	2.25	25	481000	4
	Graphite film	0.308	2.25	26.8	386724	4
	Graphite film	0.385	2.25	27.8	320923	4
	Graphene sheet	2.8	2.14	39	65087	9
	Graphene film	31	1.63	130	25727	10
	Graphene film	3.4	2.03	36.8	53409	11
	Graphene film	4	1.49	38	63926	12
	Graphene/CNT	15	1.45	57.6	26483	13
	Graphene/CNT/PVDF	100	1.77	27.58	1557	14
	Graphene paper	50	0.67	60	17910	15
	Graphene aerogel	120	0.41	85	17276	16
	Graphene foam	300	0.06	25.2	14000	17
	GCF-1400	0.483	1.63	21.72	275883	1
	Reduced graphene oxide fiber	30	0.3	31	33333	18
MXene	$Ti_3C_2T_x$	0.04	3.8	21	1381579	19
	$Ti_3C_2T_x$	0.137	3.8	33	633884	19
	Ti_2CT_x	0.094	3.8	13	363942	19
	$Ti_3C_2T_x$	1.5	2.39	45	125523	20
	$Ti_3C_2T_x$	11	2.39	68	25853	20
	$Ti_3C_2T_x$	0.94	4.3	46	120000	21
	Mxene/BC film	4	3.17	37	29141	22
	$Ti_3C_2T_x$ foam	6	0.39	32	136752	23
	MXene/Cellulose Paper	24	1.91	47	2673	24
	MXene Layer/ Cellulose Nanofiber	40	1.63	35	7029	25
	MXene Foam	6	0.39	32	136752	26
	Ti3C2Tx MXene/Graphene	1850	0.94	61	11742	27
Metal	Al foil	8	2.7	66	30555	18
	Cu foil	10	8.96	70	7812.5	18
	Cu-wrapped polymer nanofiber	1.2	1.6	45	232860	28
	CuNi-CNT foam	1500	0.23	54.6	1580	29
	Ag nanowires/PI foam	5000	0.029	35	2406	30
This Work	nMAG(PAN, 50%)	0.05	2.0	16.19	1619000	
	nMAG(PAN, 50%)	0.1	2.0	25.84	1292000	
	nMAG(PAN, 50%)	0.24	2.0	38.69	806042	
	nMAG(PAN, 60%)	0.4	2.0	40.98	512250	
	nMAG(PAN, 70%)	0.6	2.0	48.58	404832	

Supplementary References

[S1]. M. Tan, D. Chen, Y. Cheng, H. Sun, G. Chen, S. Dong, G. Zhao, B. Sun, S. Wu, W. Zhang, J. Han, W. Han, X. Zhang, Anisotropically oriented carbon films with dual-function of efficient heat dissipation and excellent electromagnetic interference shielding performances. Adv. Funct. Mater. **32**(31), 2202057. (2022). https://doi.org/10.1002/adfm.202202057

[S2]. K. Murashima, Y. Kawashima, S. Ozaki, A. Tatami, M. Tachibana, T. Watanabe, T. Harada, M. Murakami, Modified-edge-support heat treatment method of polyimide for crystalline, large-area, and self-standing ultrathin graphite films. Carbon **181**, 348-357. (2021). https://doi.org/10.1016/j.carbon.2021.05.036

[S3]. L. Peng, Y. Han, M. Wang, X. Cao, J. Gao, Y. Liu, X. Chen, B. Wang, B. Wang, C. Zhu, X. Wang, K. Cao, M. Huang, B. V. Cunning, J. Pang, W. Xu, Y. Ying, Z. Xu, W. Fang, Y. Lu, R. S. Ruoff, C. Gao, Multifunctional macroassembled graphene nanofilms with high crystallinity. Adv. Mater. **33**(49), 2104195. (2021). https://doi.org/10.1002/adma.202104195

[S4]. T. Zhou, C. Xu, H. Liu, Q. Wei, H. Wang, J. Zhang, T. Zhao, Z. Liu, X. Zhang, Y. Zeng, H. Cheng, and W. Ren, Second time-scale synthesis of high-quality graphite films by quenching for effective electromagnetic interference shielding. ACS Nano **14**(3), 3121-3128. (2020). https://doi.org/10.1021/acsnano.9b08169

[S5]. J. Ding, O. Rahman, H. Zhao, W. Peng, H. Dou, H. Chen, H. Yu, Hydroxylated graphene-based flexible carbon film with ultrahigh electrical and thermal conductivity. Nanotechnology **28**, 39. (2017). https://doi.org/10.1088/1361-6528/aa8158

[S6]. L. Peng, Z. Xu, Z. Liu, Y. Guo, P. Li, C. Gao, Ultrahigh thermal conductive yet superflexible graphene films. Adv. Mater. **29**(27), 1700589. (2017). https://doi.org/10.1002/adma.201700589

[S7]. R. Song, Q. Wang, B. Mao, Z. Wang, D. Tang, B. Zhang, J. Zhang, C. Liu, D. He, Z. Wu, S. Mu, Flexible graphite films with high conductivity for radio-frequency antennas. Carbon **130**, 164-169. (2018). https://doi.org/10.1016/j.carbon.2018.01.019

[S8]. B. Shen, W. Zhai, W. Zheng, Ultrathin flexible graphene film: an excellent thermal conducting material with efficient EMI shielding. Adv. Funct. Mater. **24**(28), 4542-4548. (2014). https://doi.org/10.1002/adfm.201400079

[S9]. S. Wan, Y. Chen, S. Fang, S. Wang, Z. Xu, L. Jiang, R. H. Baughman, Q. Cheng, High-strength scalable graphene sheets by freezing stretch-induced alignment. Nat. Mater. **20**(5), 624-631. (2021). https://doi.org/10.1038/s41563-020-00892-2

[S10]. E. Zhou, J. Xi, Y. Liu, Z. Xu, Y. Guo, L. Peng, W. Gao, J. Ying, Z. Chen and C Gao, Large-area potassium-doped highly conductive graphene films for electromagnetic interference shielding. Nanoscale **9**(47), 18613-18618. (2017). https://doi.org/10.1039/C7NR07030F

[S11]. S. Wan, Y. Chen, Y. Wang, G. Li, G. Wang, L. Liu, J. Zhang, Y. Liu, Z. Xu, A. Tomsia, L. Jiang, Q. Cheng, Ultrastrong graphene films via long-chain π-bridging. Matter **1**(2), 389-401. (2019). https://doi.org/10.1016/j.matt.2019.04.006

[S12]. Q. Wei, S. Pei, X. Qian, H. Liu, Z. Liu, W. Zhang, T. Zhou, Z. Zhang, X. Zhang, H. M. Cheng, W. Ren, Superhigh electromagnetic interference shielding of ultrathin aligned pristine graphene nanosheets film. Adv. Mater. **32**(14), 1907411. (2020). https://doi.org/10.1002/adma.201907411

[S13]. B. Zhao, C. Zhao, R. Li, S. M. Hamidinejad, and C. B. Park, Flexible, ultrathin, and high-efficiency electromagnetic shielding properties of poly(vinylidene fluoride)/carbon composite films. ACS Appl. Mater. Interfaces **9**(24), 20873-20884. (2017). https://doi.org/10.1021/acsami.7b04935

[S14]. J. Xu, R. Li, S. Ji, B. Zhao, T. Cui, X. Tan, G. Gou, J. Jian, H. Xu, Y. Qiao, Y. Yang, S. Zhang, and T. Ren, Multifunctional graphene microstructures inspired by honeycomb for ultrahigh performance electromagnetic interference shielding and wearable applications. ACS Nano **15**(5), 8907-8918. (2021). https://doi.org/10.1021/acsnano.1c01552

[S15]. L. Zhang, N. T. Alvarez, M. Zhang, M. Haase, R. Malik, D. Mast, V. Shanov, Preparation and characterization of graphene paper for electromagnetic interference shielding. Carbon **82**, 353-359. (2015). https://doi.org/10.1016/j.carbon.2014.10.080

[S16]. J. Xi, Y. Li, E. Zhou, Y. Liu, W. Gao, Y. Guo, J. Ying, Z. Chen, G. Chen, C. Gao, Graphene aerogel films with expansion enhancement effect of high-performance electromagnetic interference shielding. Carbon **135**, 44-51. (2018). https://doi.org/10.1016/j.carbon.2018.04.041

[S17]. W. Song, X. Guan, L. Fan, W. Cao, C. Wang, M. Cao, Tuning three-dimensional textures with graphene aerogels for ultra-light flexible graphene/texture composites of effective electromagnetic shielding. Carbon **93**, 151-160. (2015). https://doi.org/10.1016/j.carbon.2015.05.033

[S18]. L. Xu, H. Lu, Y. Zhou, Z. Chi, Z Li, Z. Md, Y. Dong, Y. Fu, Y. Zhu, Q. Ni, Ultrathin, ultralight, and anisotropic ordered reduced graphene oxide fiber electromagnetic interference shielding membrane. Adv. Mater. Technol. **6**(12), 2100531. (2021). https://doi.org/10.1002/admt.202100531

[S19]. M. Han, C. E. Shuck, R. Rakhmanov, D. Parchment, B. Anasori, C. M. Koo, G. Friedman and Y. Gogotsi, Beyond $Ti_3C_2T_x$: MXenes for electromagnetic interference shielding. ACS Nano **14**(4), 5008-5016. (2020). https://doi.org/10.1021/acsnano.0c01312

[S20]. F. Shahzad, M. Alhabeb,C. B. Hatter, B. Anasori, S. M. Hong, C. M. Koo, Y. Gogotsi, Electromagnetic interference shielding with 2D transition metal carbides. Science **353**(6304), 1137-1140. (2016). https://doi.org/10.1126/science.aag2421

[S21]. J Zhang, N Kong, S Uzun, A. Levitt, S. Seyedin, P. A. Lynch, S. Qin, M. Han, W. Yang, J. Liu, X. Wang, Y. Gogotsi, J. M. Razal, Scalable Manufacturing of free-standing, strong $Ti_3C_2T_x$ MXene films with outstanding conductivity. Adv. Mater. **32**(23), 2001093. (2020). https://doi.org/10.1002/adma.202001093

[S22]. Y. Wan, P. Xiong, J. Liu, F. Feng, X. Xun, F. M. Gama, Q. Zhang, F. Yao, Z. Yang, H. Luo, Y. Xu, Ultrathin, strong, and highly flexible $Ti_3C_2T_x$ MXene/bacterial cellulose composite films for high-performance electromagnetic interference shielding. ACS Nano **15**(5), 8439-8449. (2021). https://doi.org/10.1021/acsnano.0c10666

[S23]. J. Liu, H. Zhang, R. Sun, Y. Liu, Z. Liu, A. Zhou, Z. Yu, Hydrophobic, flexible, and lightweight MXene foams for high-performance electromagnetic-interference shielding. Adv. Mater. **29**(38), 1702367. (2017). https://doi.org/10.1002/adma.201702367

[S24]. W. Cao, F. Chen, Y. Zhu, Y. Zhang, Y. Jiang, M. Ma, F. Chen, Binary strengthening and toughening of MXene/cellulose nanofiber composite paper with nacre-inspired structure and superior electromagnetic interference shielding properties. ACS Nano **12**(5), 4583-4593. (2018). https://doi.org/10.1021/acsnano.8b00997

[S25]. B. Zhou, Z. Zhang, Y. Li, G. Han, Y. Feng, B. Wang, D. Zhang, J. Ma, C. Liu, Flexible, robust, and multifunctional electromagnetic interference shielding film with alternating cellulose nanofiber and MXene layers. ACS Appl. Mater. Interfaces **12**(4), 4895-4905. (2020). https://doi.org/10.1021/acsami.9b19768

[S26]. J. Liu, H. Zhang, R. Sun, Y. Liu, Z. Liu, A. Zhou, Z. Yu, Hydrophobic, flexible, and lightweight MXene foams for high-performance electromagnetic-interference shielding. Adv. Mater. **29**(38), 1702367. (2017). https://doi.org/10.1002/adma.201702367

[S27]. Y. Chen, X. Zheng, J. Cai, G. Zhao, B. Zhang, Z. Luo, G. Wang, H. Pan, and W. Sun, Sulfur doping triggering enhanced Pt–N coordination in graphitic carbon nitride-supported Pt electrocatalysts toward efficient oxygen reduction reaction. ACS Catal. **12**(12), 7406-7414. (2022). https://doi.org/10.1021/acscatal.2c00944

[S28]. Z. Zeng, F. Jiang, Y. Yue, D. Han, L. Lin, S. Zhao, Y. B. Zhao, Z. Pan, C. Li, G. Nyström, J. Wang, Flexible and ultrathin waterproof cellular membranes based on high-conjunction metal-wrapped polymer nanofibers for electromagnetic interference shielding. Adv. Mater. **32**(19), 1908496. (2020). https://doi.org/10.1002/adma.201908496

[S29]. K. Ji, H. Zhao, J. Zhang, J. Chen, Z. Dai, Fabrication and electromagnetic interference shielding performance of open-cell foam of a Cu–Ni alloy integrated with CNTs. Appl. Surf. Sci. **311**, 351-356. (2014). https://doi.org/10.1016/j.apsusc.2014.05.067

[S30]. J. Ma, K. Wang, M. Zhan, A comparative study of structure and electromagnetic interference shielding performance for silver nanostructure hybrid polyimide foams. RSC Adv. **5**(80), 65283-65296. (2015). https://doi.org/10.1039/C5RA09507G